Kinetics of a polysoap collapse

Nam-Kyung Lee and Cameron F. Abrams

Citation: The Journal of Chemical Physics **121**, 7484 (2004); doi: 10.1063/1.1793151
View online: http://dx.doi.org/10.1063/1.1793151
View Table of Contents: http://scitation.aip.org/content/aip/journal/jcp/121/15?ver=pdfcov
Published by the AIP Publishing

Kinetics of a polysoap collapse

Nam-Kyung Lee
Department of Physics, Institute of Fundamental Physics, Sejong University, Seoul, South Korea; Institut Charles Sadron, 67083 Strasbourg Cedex, France; and Max-Planck-Institut für Polymerforschung, Ackermannweg 10, 55128 Mainz, Germany

Cameron F. Abrams
Department of Chemical Engineering, Drexel University, Philadelphia, Pennsylvania 19104

(Received 21 June 2004; accepted 22 July 2004)

We study the dynamics of collapse of a polysoap by means of large-scale molecular dynamics simulation and scaling arguments. A polysoap consists of a hydrophilic backbone and hydrophobic side chains attached at regular intervals along the backbone. In selective solvent conditions, the hydrophobic components aggregate, forcing the hydrophilic backbone to form loops anchored at the surface of the core, ultimately forming a micelle. The kinetics of polysoap collapse includes two major mechanisms: (1) early aggregation of the hydrophobic side chains controlled by first-order kinetics whose rate constant is given by a contact probability and (2) coalescence into larger clusters which requires activation to overcome energy barriers due to excluded volume repulsions between intermediate micelle coronas. In the late stage, the energy barrier is increasing as $p^{3/2}$, with p the number of aggregated side chains in an intermediate micelle. The corresponding late-stage rate constant decays exponentially as $\sim\exp(-p^{3/2})$. © *2004 American Institute of Physics.*
[DOI: 10.1063/1.1793151]

I. INTRODUCTION

The process of polymer collapse has attracted much attention[1–11] for last few decades, motivated primarily by its partial analogy to protein folding. On the theoretical side, many models were proposed based on de Gennes seminal ''*expanding sausage*'' model.[1] Recently, we have shown that computer simulation of generic polymer models in explicit solvent has become a powerful means of discriminating among these models. We argued that homopolymer collapse is dominated by a deterministic streamlining process where larger and larger chain sections with a pearl-necklace structure align, while the overall end-to-end distance remains constant, until, in a last step, the resulting dumbbell collapses. This theory is supported, at the level of time-dependent structural evolution, by large-scale simulations.[12]

A coil-to-globule transition occurs in a heteropolymer provided that there is a sufficient number of hydrophobic monomers. Similar to homopolymer collapse, the collapse of a chain bearing hydrophobic residues in close proximity to each other along the backbone is a deterministic process. However, in contrast, aggregation among hydrophobic segments which are separated by hydrophilic segments depends on the dynamics of the connecting hydrophilic parts of the polymer chain which are ultimately forced into loops. Hence, these kinetics are controlled by diffusion through antagonistic energy barriers.

The collapse dynamics of a heterogeneous polymer has some connection to the early stage of protein folding.[13] It has been suggested that protein folding is a two-step process: ''collapse'' into a dense phase followed by ''folding'' to form the specific internal structure. The first process is fast compared to the second, in which the arrangement of the internal chain segments involves a slow process of overcoming several energy barriers. Moreover, recent experiments suggest that the first stage is also subject to energy barriers, regardless of whether the second stage (specific folding) is thermodynamically favored or not.[14] This early collapse process likely resembles the formation of a heteropolymeric micelle[15,16] in the sense that the contact probability of reacting hydrophobic clusters is controlled by the statistics of the connecting hydrophilic segments. There is therefore considerable grounds for pursuing a better understanding of heteropolymer collapse.

In this contribution, we consider the kinetics of the collapse of a polysoap molecule. A polysoap is defined as an amphiphilic polymer which, under the appropriate solvent conditions, has a soluble backbone and insoluble side chains.[16,17] We consider a polysoap consisting of N hydrophilic backbone monomers onto which hydrophobic side chains of length M are attached with equal spacing s [Fig. 1(a)]. By collapse, we refer to the process by which the hydrophobic side chains in an open polysoap molecule aggregate to form a single core dressed by backbone loops, an object we refer to as a micelle [Fig. 1(c)]. The purpose of this paper is to present a complete picture that can capture the major aspects of the kinetics of this process using scaling arguments and computer experiments.

The simulations described here include explicit solvent particles and use no thermostat, guaranteeing a proper kinetic description. Past simulation studies of self-assembly of amphiphilic comb-graft heteropolymers in vacuum demonstrate qualitative aspects of collapse pathways, including the possibility of metastable states.[18–20] However, because they are primarily stochastic, none of these simulations allowed for an estimation of the dependence of characteristic times on

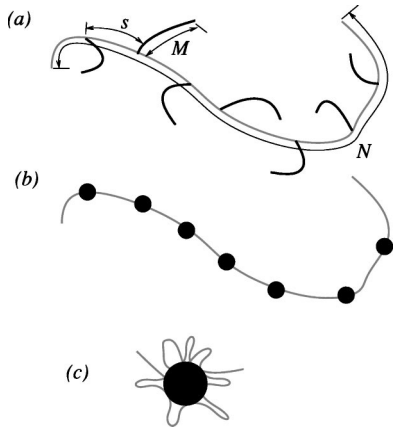

FIG. 1. (a) Schematic representation of a polysoap comprised of hydrophobic side chains and hydrophilic backbone. (b) Schematic of a polysoap for which $M \ll s$, immediately after self-collapse of side chains, prior to sticker aggregation and micelle formation. (c) A collapsed polysoap micelle.

topological parameters. Our simulations are intended to fill this current gap, providing a more rigorous test of the scaling theory.

We intend to provide a qualitative estimation of the characteristic times of collapse. The kinetics clearly depend on the topological parameters s, M, and N in a nontrivial manner. Our theory focuses on two major aspects of the topology: (a) the relative size of the side chains to backbone spacer, M vs s, and (b) the number of side chains, N/s.

The rest of this manuscript is organized as follows: In Sec. II, we describe the molecular dynamics simulations. In Sec. III, we present a theory of the kinetics of polysoap collapse based on scaling arguments. In Sec. IV, we draw comparisons between what is observed in the simulations and what is predicted by the theory. In Sec. V, we summarize the mechanisms of collapse in a kinetic phase diagram. We conclude in Sec. VI.

II. SIMULATION TECHNIQUES

The collapse of a polysoap in selective solvent was simulated using molecular dynamics (MD) with explicit solvent. Systems considered are shown in Table I. The prototype system is a single polymer backbone of length N type-B monomers, onto which side chains of length M type-A monomers are grafted at intervals of s. This molecule is immersed in a solvent of N_s simple type-B solvent particles, contained in a cubic box. The total particle number density ρ is $0.85\sigma^{-3}$ in all cases. All pairs of particles interact via

TABLE I. Summary of simulations: N, backbone length; s, backbone spacer length between grafting points; M, side-chain length; N_s, number of solvent particles; "#" number of independent trajectories.

N	s	M	N_s	#
53	5	5	15 000	40
103	10	5	25 000	40
203	20	5	50 000	20

standard Lennard-Jones potentials. For "good" solvent conditions, all particles interact via the fully repulsive Weeks-Chandler-Andersen (WCA) potential:[21]

$$U_{\mathrm{WCA}}(r)=\begin{cases} 4\epsilon\left[\left(\frac{\sigma}{r}\right)^{12}-\left(\frac{\sigma}{r}\right)^{6}+\frac{1}{4}\right], & r<2^{1/6}\sigma \\ 0, & r>2^{1/6}\sigma. \end{cases} \tag{1}$$

For "selective" solvent conditions, the AA and BB pair interactions are attractive, treated with the full Lennard-Jones potential, $U_{LJ}(r)$, with a well depth ϵ of 1.0, cut off at $r=r_c=2.5\sigma$, while the AB pair interaction is kept as the repulsive $U_{\mathrm{WCA}}(r)$. A shift is added to U_{LJ} such that $U_{LJ}(r_c)=0$:

$$U_{LJ}(r)=\begin{cases} 4\epsilon\left[\left(\frac{\sigma}{r}\right)^{12}-\left(\frac{\sigma}{r}\right)^{6}-\left(\frac{\sigma}{r_c}\right)^{12}+\left(\frac{\sigma}{r_c}\right)^{6}\right], & r<r_c \\ 0, & r>r_c. \end{cases} \tag{2}$$

This simple prescription was used previously in order to drive phase separation in homopolymer collapse simulations.[6,12,22] Particles are connected to each other along the backbone of a chain using via the finite extensible nonlinear elastic (FENE)/WCA potential[23] with the standard values $a=30.0\epsilon$ and $R_0=1.5\sigma$:[23]

$$U_{\mathrm{FENE/WCA}}(r)=U_{\mathrm{WCA}}(r)+U_{\mathrm{FENE}}(r)$$

$$U_{\mathrm{FENE}}(r)=-\frac{a}{2}R_0^2\ln\left[1-\left(\frac{r}{R_0}\right)\right]. \tag{3}$$

The particle Newtonian equations of motion are integrated using the velocity-Verlet algorithm, with a time step Δt of $0.004t_0$, where $t_0=\sqrt{m\sigma^2/\epsilon}$ and $m=1$. We measure the fluctuating temperature in units of ϵ/k_{B}.

The procedure for a single collapse trajectory is as follows. First, the backbone length N, side-chain length M, and spacing s are chosen. The cubic box size L is determined such that $L \gtrsim 2R(N)$, where $R(N)$ is the root-mean-squared end-to-end distance of a linear chain of N monomers in good solvent, determined by short MD simulations. The initial backbone conformation was generated by growing a nonreversal random walk (NRRW) of length N and step length $l=0.97\sigma$. Then, side chains are grown as NRRWs of length M beginning at every sth monomer on the backbone. Then the N_s solvent particles are added at random locations in the box. Particle overlaps are then removed using a previously detailed warmup technique,[24] which incrementally increases the excluded volume diameter of the particles from zero to its full value over 5 000 MD time steps in good solvent conditions. During this phase, a Langevin-type thermostat with friction $\Gamma=5.0t_0^{-1}$ and a set-point temperature $T_L=0.92$ is employed.[23]

Immediately following the warmup, designated $t=0$, the quench into selective solvent conditions is performed via instantaneously "switching on" attraction in AA and BB pairs (i.e., AA and BB pair interactions are switched from U_g to U_{LJ}), and switching off the thermostat. This NVE MD integration is typically run for several thousand t_0 with a time step $\delta t=0.004t_0$, until the polysoap has fully collapsed into

TABLE II. Summary of simulations: s, backbone spacer length; t_c, mean collapse time; δt_c, standard deviation of t_c; T, mean temperature; δT, standard deviation of T as a percentage of T. The entry in the last column indicates the class of early stage kinetics (DC: diffusion controlled).

s	t_c (t_0)	δt_c (t_0)	T	δT (%)	
5	523.3	245.4	0.992	0.4	DC
10	2175.0	1257.0	0.990	0.3	Marginal
20	14000.0	⋯	⋯	0.3	Marginal

a single micelle. The collapse is monitored using the radius of gyration of the collection of side-chain monomers, $R_{g,aa}^2$, as a function of time:

$$R_{g,aa}^2 = \frac{1}{2(MN/s)^2} \sum_{ij \in A} (\mathbf{r}_i - \mathbf{r}_j)^2. \tag{4}$$

Note that MN/s is the number of A-type monomers. During this integration, configuration snapshots are stored every t_0 for the first $100t_0$, and every ten t_0 thereafter, for later analysis. All simulations were run on AMD Athlon MP2200+ processors. The largest runs with $s=20$ were run in parallel on four hardwared interconnected processors using a domain decomposition algorithm.[25] Forty independent collapses were simulated for $s=5$ and 10, and 20 for $s=20$, each beginning with a unique polysoap conformation.

An important observable from the simulations is the time-dependent cluster size distribution of side-chain monomers, $n_x(t)$, where x is the number of side chains in a cluster. Two monomers belong to the same cluster at time t if (a) they are members of the same side chain (which means they are always members of the same cluster) or (b) they are within 1.2σ of each other.

During the course of a typical collapse simulation, the time-averaged temperature (sampled every $1t_0$) fluctuates around $\langle T \rangle = 1.0$ by about 0.5%, as indicated in Table II. For simulations of this length and containing relatively large numbers of particles, it is therefore not necessary to use a thermostat to maintain the desired temperature of $T=1.0$. The only consideration is setting the temperature in the warmup-phase slightly below 1.0, because instantaneously switching pair potentials at quench introduces more kinetic energy into the system. The warmup-phase set-point temperature of 0.92 was found by trial and error to lead to an average temperature of about 1.0 in the subsequent *NVE* simulations.

III. THEORY: KINETICS OF POLYSOAP COLLAPSE

Our theory describes a two-stage collapse mechanism of excluded volume chain. In the early stage of internal cyclization, described in Sec. III A, isolated side chains begin to aggregate based on their contact probability. In contrast to the collapse process of a homopolymer, which is mainly deterministic, the process of polysoap collapse depends on the statistics of the hydrophilic backbone conformations, which remains swollen during the process of micelle formation. The collapsed stickers have to overcome the excluded volume barrier against internal pair contact to aggregate. For large spacers, these excluded volume barriers are already relevant in the early-stage kinetics. The further aggregation of side chains brings connecting backbone chains together and localizes them on the surface of a growing hydrophobic core. During these later stages of collapse, described in Sec. III B, as more side chains enter the core, the surface becomes more crowded by backbone chains (Daoud-Cotton regime[26]). Energy barriers become very large in thermal unit in the later stage.

A. Early stages of collapse

The kinetics of intramolecular reactions involving multiple reactive groups (generically, ''stickers;'' for polysoaps, ''side chains'') on flexible backbones falls into two major categories: Mean field (MF) and diffusion controlled (DC).[27,28] The intramolecular cyclization kinetics between *two* reactive groups in dilute solution has previously been considered.[27–30] The cyclization controls the kinetics of a chain with a few stickers which do not go through the Daoud-Cotton regime.[26] Here, we discuss intramolecular reactions among *many* reactive groups on the same molecule. We distinguish between MF and DC depending on the ratio of the distance between the grafting points s to the sticker length M. We demonstrate that marginal kinetics (between MF and DC) describes the early stages of collapse *when the sticker size is negligible compared to the spacer length*, or $s \gg M$.

There are also other regimes describing the small spacer size or weakly collapsed stickers, which appear in some of our simulation runs. We consider the collapse kinetics with larger size stickers, $s \sim M$, in Appendix B. For weaker stickers of finite size, additional channels open by sticker fluctuation, which leads to DC. For large stickers, we show that kinetics is MF due to the initial overlap of stickers.

We restrict our analysis in this section to the case that the backbone spacer length between grafting points is much larger than the size of the side chains: $s \gg M$. We also assume that side-chain stickers are self-collapsed immediately after solvent quench and the size of stickers, $r_{sticker}$, is negligible. This is valid if the self-collapse time of stickers of length M is $t_{coll} \sim M/\tau$, which is smaller than the Zimm relaxation time of the spacer ($t_s \sim s^{3\nu}$). We consider any pair of stickers in the polysoap, which may be two chain ends, one end and one interior sticker, or two interior stickers, connected by a flexible linear chain segment of length s. The typical distance between them is $R_s \sim s^{\nu}$, where ν is taken to be the good-solvent scaling exponent approximately equal to 0.59.

The mutual distance between the members of any pair of stickers is governed by diffusion. Modes with wavelengths longer than the contour length of the considered chain section do not affect the mutual distance between the stickers. For times larger than the spacer relaxation time t_s ($\sim s^{3\nu}$ in Zimm dynamics), the friction thus starts to saturate to that of a spacer. The long-time diffusion rate is thus inversely proportional to the geometrical size of the spacer when hydrodynamics is taken into account. Here and below we measure time and length in units of $\tau_0 = \eta_0 b^3/k_B T$ and monomer size b, respectively, where η_0 is the solvent viscosity.

For short times $t < t_s$, as the correlated contour lengths $[s'(t) < s]$ which diffuse together grow with time, the vis-

cous friction of the moving object also grows. In Zimm dynamics, the hydrodynamic friction is proportional to the geometric size of the correlated segment. The resulting time-dependent fluctuation of the mean-squared displacement is therefore $\delta R(t) \sim t^{1/\alpha}$ with $\alpha = 3$.[31] In the long-time limit, $\delta R(t)$ becomes saturated at $x_{eq} \sim s^{\nu}$ for the time larger than t_s:

$$\delta R(t) \sim \begin{cases} (t/t_s)^{1/\alpha}, & t < t_s \\ x_{eq} \sim s^{\nu}, & t \geqslant t_s. \end{cases} \tag{5}$$

As the explored volume by a spacer $[\delta R(t)]^d$ is marginally compact, whether kinetics is MF or DC depends on the value of local reactivity Q.

To estimate Q we need a model for the aggregation of two collapsed stickers upon contact. There is no energy barrier that would prevent aggregation upon contact in our model. (There may be, of course, barriers to bring stickers to within the contact distance of each other.) Each sticker globule may be thought of as a dense array of Gaussian thermal blobs of $g \sim 1/\tau^2$ monomers and radius $\xi \sim b/\tau$ with τ being the temperature quench depth. Sticking is irreversible after a few thermal blobs have reorganized in the contact zone between the globules, this requires about the relaxation time of a thermal blob, $Q \sim \tau^{-3}$. In the collapse process, Q is inversely proportional to the relaxation time of a thermal blob, τ^3. The retained characteristic time is shorter than the longest time for the shape relaxation of the sticker dimer $(\eta r_{sticker}/\gamma)$ driven by the surface tension $\gamma \sim \tau^2$, by a factor $(M/g)^{1/3}$ only. As the condition $Qt_s > 1$ holds, the kinetics is DC.

However, for larger spacers $[\nu\theta \ln(s) > 1]$, the excluded volume barrier is relevant and the reaction should occur through a barrier of size $\sim k_B T \ln(s^{\nu} b/r_{sticker})^{\theta_a}$. Here, θ_a $(a = 0,1,2)$ is the des Cloizeaux's contact exponent[33] which depends on the location of the considered segment along the chain (see Appendix A for an explanation of contact exponents). The number fraction of the reacted stickers, $r(t)$, at time t after solvent quench is increasing by the rate of making contacts between stickers. If kinetics is MF, stickers explore space in a dilute fashion; hence all degrees of freedom of each spacer are thermalized before the aggregation of sticker pairs (i.e., the ''closure approximation'').[29] Then the reaction probability is given by the product of *equilibrium contact probability* and Q. Hence, the rate constant for a pair reaction, $k^{MF} \approx dr(t)/dt$, is

$$k^{\mathrm{MF}} = Q\left(\frac{r_{sticker}}{R_s}\right)^{d+\theta_a} \approx s^{-\nu(d+\theta)}. \tag{6}$$

Mean field requires $Q(r_{sticker}/b)^d < 1$ in order for all spacer configurations to be explored prior to sticking. From a formal point of view, this condition is never met with the previous estimate $Q \sim \tau^3$ for strong stickers comprising many thermal blobs.

For larger Q, stickers diffuse toward each other against the spacer excluded volume repulsion and stick upon first contact. Assuming DC, the unreacted configurations do not follow equilibrium statistics. The probability of unreacted sticker globules vanishes at contact and should be thermalized far enough from contact region. The probability leads from the equilibrium value $P_e(r = r_{sticker}) = [(r_{sticker}/b)^{d-1}/s^{\nu d}](r_{sticker}/s^{\nu} b)^{\theta}$ to 0 over a distance of $r_{stickers}$. The friction of the short mode over a globule radius is $\eta_{glob} \sim 6\pi\eta_0 r_{stickers}$. The corresponding kinetic constant k^{DC} is the product of the probability gradient and $k_B T/\eta_{glob}$. We write

$$k^{\mathrm{DC}} = (r_{sticker}/b)^{\theta_a} s^{-\nu(d+\theta_a)} \approx s^{-\nu(d+\theta_a)}. \tag{7}$$

The fact that k^{MF} and k^{DC} have similar s dependence just reminds us that the kinetics is marginal. In short, although the kinetics is generally marginal, our simulation results (which employ a deep solvent quench) seem to favor DC. In the subsequent section, Q is therefore omitted.

The overall kinetic rate k^M includes the contributions from all pairs regardless of whether the pair kinetics is MF or DC. Let us define $P(m_1, m_2)$ as the probability for a given sticker at m_1 to make contact with any other sticker at position m_2. The distance between two stickers is $R \sim [(m_2 - m_1)s]^{\nu}$ if we neglect the sticker size. As stickers are positioned along the backbone spaced by $\delta m s$ $(\delta m = m_2 - m_1 = 1,2,3,\ldots)$, the probability to react for a given sticker at m_1 in a given time interval δt is the sum over all pair distributions,

$$k^{\mathrm{M}}(m_1)\,\delta t = \sum_{m_2} P(m_1, m_2), \tag{8}$$

and the number of unreacted stickers is

$$n_1(t) = n_0 \prod_{\delta t} [1 - k^{\mathrm{M}}(m_1)\,\delta t] \sim n_0 \exp\left[-\int k^{\mathrm{M}} dt\right]. \tag{9}$$

As m_1 can correspond to any sticker, we simply write $k^M(m_1)$ as $k^M(m)$ to obtain the exponential decay of unreacted stickers as a function of t with kinetic rate k^{M}. Hence, the aggregation is dominated by first-order reaction kinetics:

$$\frac{dn_1(t)}{dt} = -k^{\mathrm{M}}(m) n_1(t). \tag{10}$$

In the limit of a chain with infinitely many repeating units $(n_0 \to \infty)$,

$$\begin{aligned} &n_1(t) = n_0 \exp(-k_{\infty}^{\mathrm{M}} t), \\ &k_{\infty}^{\mathrm{M}} = s^{-\nu(d+\theta_a)} \zeta[\nu(d+\theta_a)], \end{aligned} \tag{11}$$

where $\zeta(x) = \Sigma_n 1/n^x$ is the Riemann Zeta function.

B. Late stages of collapse

The free energy of the micelle consisting of p repeating blocks is

$$F_m/k_B T = 4\pi\gamma R_c^2 + k_B T p^{3/2} \ln(s^{3/5}/M^{1/3} p^{2/15}), \tag{12}$$

where $R_c = (pM)^{1/3}$ is the core size. The second term of the free energy representing the stretched chains in the corona is estimated by the Daoud-Cotton model in a good solvent[26] for the star geometry.[34] The optimal micelle size p^* is given by the interplay between (a) the surface energy between collapsed side chains and solvent particles and (b) the stretching energy of backbone chains in the coronas. The larger the surface tension, the larger is the aggregation number. By

minimizing $F_m(p)/p$, Daoud and Cotton found that the optimal aggregation number p^* should satisfy the following condition:[26]

$$p^* = M^{4/5}\left(\frac{\gamma}{k_B T \ln[s^{3/5}(p^*)^{-2/15}M^{-1/3}]}\right)^{6/5}. \tag{13}$$

Note that p^* is mainly determined by M and the surface tension γ. We disregard the weak logarithmic dependence on s below. If the number of repeating units is larger than the optimal size of micelle, $N/s > p^*$, the final number of micelles can be greater than one. During collapse, as aggregation among side chains proceeds, the number of aggregated side chains in a cluster, $p(t) < p^*$, grows. The accumulated number of backbone strands on surface of the cluster is also $p(t)$. p^* defines a limit in cluster size depending on the side-chain length and surface energy. One may think of the quench into selective solvent conditions as an instantaneous shift of p^* to some finite number $p^* > 1$. The clusters start growing until their average size reaches p^*.

For shorter spacers [$\nu\theta \ln(s) < 1$], it is useful to introduce overlap aggregation number p^o. If the number of loops of backbone chains tethered to the surface of the cores exceeds the overlap aggregation number $p^o \leqslant p^*$, loops start overlapping and become stretched. From the condition of the onset of the semidilute surface regime, $\sigma > \sigma^*$, we obtain the onset of the overlap in aggregation number p^o, provided that core size is comparable to the size of a spacer:

$$p^o = (2\pi)^3 M^2 (s/2)^{-6\nu}. \tag{14}$$

As the cluster size grows, the backbone chains become crowded on the surface of the existing clusters, and in order to bring another side chain into the core, it must penetrate the surrounding "cloud" of backbone loops and overcome a corresponding entropic penalty. The later stage is hence characterized by such free energy barriers, and we denote this kinetic regime energy barrier dominated (EB). For given sticker size M, the onset of energy-barrier-dominated regime t_{EB} occurs earlier for large s:

$$t_{EB} \sim p^o / k^M \sim s^{-(6-d-\theta_a)\nu}. \tag{15}$$

For large spacer length [$\nu\theta \ln(s) < 1$], the onset is actually at $p^o = 2$ and the EB kinetics covers the early marginal kinetic regime.

We now follow the steps of Daoud-Cotton starlike micelle model[26] to estimate the energy barrier related to cluster coalescence in the intermediate stages. We note that the kinetics of adsorption of block copolymers from the micelle phase has been treated by Johner and Joanny in a similar analysis.[35] The relaxation time for the aggregated segments and attached backbone is much shorter than the time scale for another segment to overcome the energy barrier and therefore become adsorbed. In such a way, we can obtain the growth rate of clusters $dp(t)/dt$ using quasiequilibrium energy barriers at given $p(t)$. Taking into account interactions of backbone chains in the coronas, the optimal size of the cluster can be estimated to be p^*. As the micelle grows, following the Daoud-Cotton model, the free energy stored in the stretched part of the backbone chain in the micelles consisting of p repeating unit is given as

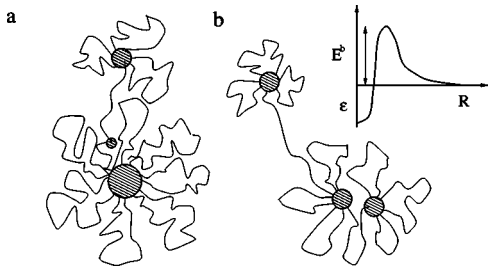

FIG. 2. The energy barrier controlled kinetic modes of polysoap collapse. (a) The larger clusters are growing by absorbing single-side-chain cluster one after another (SM). For $p > p^*$, this is part of the slow mode. (b) Two clusters merge directly below p^* (ME). The potential of a micelle as a function of the distance from the micelle core has a well depth $\sim M\gamma_s$ and screening energy barrier $\sim p^{3/2}$.

$$F(R) = k_B T p^{3/2} \ln(R/R_c), \tag{16}$$

where R is the micelle size and $R_c \sim (pM)^{1/3}$ is size of the hydrophobic core. If $R_c \ll R$, $R \approx (s^3 p)^{1/5}$.

There are several kinetic modes. In order to bring p_2 side chains to the cluster consisting of p_1 side chains, a total of $p_1 + p_2$ spacers must be brought together. The coronas in both micelles repel each other via repulsive excluded volume interactions. The interaction energy becomes maximum when two micelle cores are brought to within the distance of contact. The entropic penalty of arranging the coronas in the limited fraction of the solid angle $4\pi p_i/(p_1+p_2)$ increases the free energy density. The maximum stretching energy of coronas is $E^b(p_1,p_2) = k_B T (p_1+p_2)^{3/2} \ln(R'/R_c')$. With $p_t = p_1 + p_2$, the corresponding rate constant is

$$k(t) \sim \frac{R_c'}{R'} \exp[-E^b(p_t)/k_B T], \tag{17}$$

where R_c' is the effective core size on contact $\sim 2R_c$ and new micelle size $R' \sim s^{3/7}(p_1+p_2)^{1/5}$ from the condition that the micelle is a space-filling packing of blobs of backbone monomers as large as R'.

We consider two major relaxation processes of cluster growth, depicted in Fig. 2. Clusters of sizes p_1 and p_2 aggregate into a product cluster with size $p_t = p_1 + p_2$. The first mode prescribes that a large cluster (p_1) grows by absorbing side chains ($p_2 = 1$) one after another, i.e., the single-side-chain exchange mode (SE). The associated duration of the metastable cluster of size p_1 is

$$t^{SE}_{p_1 \to p_t = p_1 + 1} = \left(\frac{R}{R_c}\right)^{(p_1+1)^{3/2}}. \tag{18}$$

The second kinetic mode is the combining of two similarly sized clusters, i.e., multiple-side-chain exchange mode (abbreviated by ME below). Clearly, after all single clusters are absorbed, only the second mode can occur. Two micelles can merge if the combined aggregation number, $2p$, is less than p^*, despite a large energy barrier. The density of the half space becomes multipled by p_t/p_1 at the point of contact between cores. The interacting energy is maximum when two equally sized micelles bring their cores in contact. The corresponding energy barrier is $(2p)^{3/2} k_B T$ to within power law accuracy. Hence,

$$t_{p\to 2p}^{ME}=\left(\frac{R}{R_c}\right)^{(2p)^{3/2}}. \tag{19}$$

Below $p_t<p^*$, $t^{single}\approx t^{multi}$ for the same final state p_t. For a long chain, for which the equilibrium state is understood to be a chain of micelles, the final stage of the relaxation into the final equilibrium micelle size distribution is a collective relaxation of many established micelles. We denote this kinetic regime "CR" (CR—collective relaxation). For aggregation of $p_1+p_2\to p_t>p^*$, the mass distribution between clusters requires dissolving of some existing micelle clusters. The resulting final clusters are those with optimal cluster size p^* and the other $p'=p_t-p^*$. Larger clusters can grow further at the expense of small micelles via the first mode. This slow mode is a two-step process: (1) first removing a single-side-chain cluster to the bulk from smaller micelle and (2) then bringing it into the larger cluster.

The SE mode dominates early EB regime. The decay rate of the unreacted side chain, $\lambda=-d[n_1(t)/n_0]/dt$, slows down at the onset of the semidilute surface regime. Provided that the cluster growth is dominated by the single-side-chain exchange process until the micelle size p becomes p^*, we write $n_1(t)=-p(t)$ and the flux of adsorbing single side-chain clusters is proportional to $e^{-p^{3/2}}$. Assuming that the fluctuation in $p(t)$ is small, we approximate the kinetic rate to be

$$\frac{d\tilde{p}}{dt}=\left(\frac{R}{R_c}\right)^{-\tilde{p}^{3/2}}, \tag{20}$$

where $\tilde{p}$ stands for the average value of $p(t)$ at given time. After all single side chains are absorbed into clusters, the cluster is growing either by ME or CR. The duration at each metastable stage also becomes longer as the cluster size grows. The final stage of collapse for two clusters to one takes the longest because the energy barrier increases as a power of p.

IV. SIMULATION RESULTS

Here, we turn to a discussion of our simulation results in the light of a few of our major theoretical predictions. In the early stages of collapse, we indeed observe exponential decay of the number of single-side-chain clusters $n_1(t)$ (clusters for which $p=1$) as suggested from Eq. (10), which appears linear decay in log-linear plot of $n_1(t)$ vs time t. In the inset of Fig. 3(a), we show the early time evolution of $n_1(t)$, the number of singe-side-chain clusters, for collapsing polysoaps with spacer lengths $s=5$, 10, and 20. Exponential decay is apparent in the early stages of collapse in case of $s=10$, 20. However, for $s=5$, the rate constant is the function of time; there is no clear linear regime. This implies that there is another kinetic channel of cluster aggregation besides DC through barriers. As the sticker size is as large as spacer size, the picture of point contact in DC obviously fails. (We discussed the influence of the large sticker size in detail in Appendix B.) Note that in the very beginning of the collapse, the initial conformations determine kinetic pathways. This is manifest in the rapid decay of $n_1(t)$ in $t<10t_0$ due to the initial overlaps of the extended side chains for all s's considered.

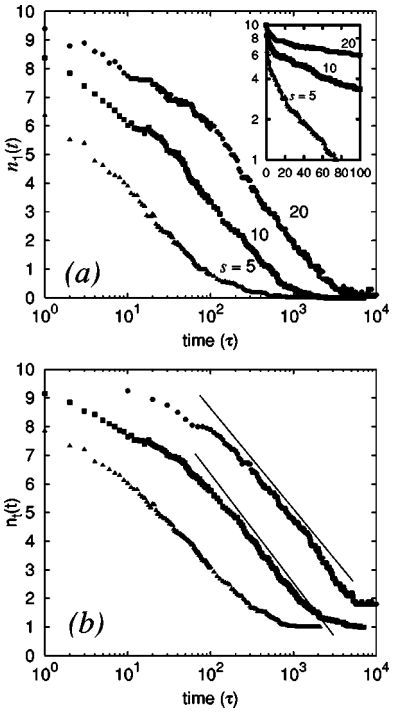

FIG. 3. Simulation results: (a) Time evolution of number of unreacted single-side-chain clusters, $n_1(t)$, for backbone spacer lengths $s=5$, 10, and 20. Time is measured in units of t_0. Inset shows early decays of n_1. Notice that $n_1(t)$ decays exponentially in the early stage ($10<t<100t_0$) for $s=10$ and 20, and logarithmically in the later stages of coalescence. (b) Time evolution of total number of clusters, $n_t(t)$, for the three backbone spacer lengths.

To compare qualitatively with our scaling theory, we computed the first-round clusterization time $t_{1/2}$ in a good solvent. We expect, on average, each cluster has reacted after time $t_{1/2}$. Hence, $t_{1/2}$ is the mean time required to halve the number of clusters. Equation (10) gives the estimate $t_{1/2}\sim \ln 2/k^{\mathrm{M}}$. The main contribution to this reaction is from pairs with the shortest contour distance separating their members, i.e., $\delta m_{min}=1$. Taking into account the good solvent contact exponents (θ_a) (Ref. 33) and the leading δm dependent term of k^M from Eq. (10), the estimated time for the first-round clusterization is $s^{\nu(d+\theta_a)}$. Therefore the time needed to halve the number of the unreacted side chains can be approximated as a cyclization time involving neighboring pairs (those separated by the distance s) along the backbone and thus inversely proportional to the kinetic rate k_M [see Eqs. (6) and (7)]:

$$t_{1/2}\sim 1/k^M\sim s^{9/5+\nu\theta_a}. \tag{21}$$

Considering $\nu\theta_a=0.2\sim 0.32$ (depending on which des Cloizeaux exponent is chosen),[33] we thus find $t_{1/2}\sim s^{2.12}$. Here, we assumed that internal sticker pair makes the dominant contribution, so that $\theta_a\approx\theta_2$. The contribution from pairs with larger $\delta m>1$ to the reaction rate, which is about $1-1/\zeta(2)\approx 0.39$, is not negligible. Nonetheless the recur-

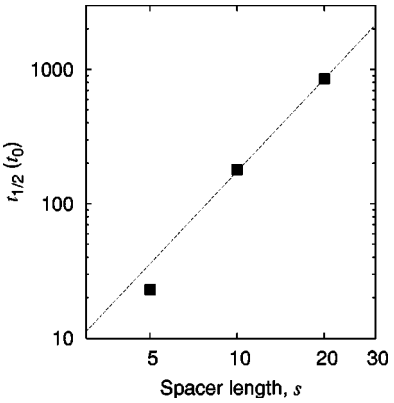

FIG. 4. Simulation results: Dependence of first-round cyclization time $t_{1/2}$, measured in units of t_0, on spacer length s. Dashed line is a best fit of $t_{1/2} \sim s^{\nu_{sim}}$ with $\nu_{sim}=2.3$.

sive reactions from the shortest pairwise coalescence precede any of the reactions involving pairs separated by longer distances.

In Fig. 4, we plot $t_{1/2}$, measured from simulations of polysoaps with different spacings s and fixed M and N/s. It is important to note that $t_{1/2}$ is computed as the time at which the average *number* of clusters, regardless of size, is 5. Therefore, $t_{1/2}$ from the simulations is sensitive to early modes of reaction other than the simplest case of single-side-chain aggregation used in our approximation in Eq. (21). We observe that $t_{1/2}$ grows with respect to $s^{\nu_{sim}}$ with $\nu_{sim} \approx 2.3$, close to our prediction of $\nu=2.12$. The discrepancy is due in part to the approximation that only aggregation of pairs of unreacted side chains contributes to the early clusterization. Though it is the major mechanism, other reaction modes come into play early in the process as well, such as single-side-chain addition to a cluster of two or three side chains. Such higher-order modes appear earlier for shorter values of s, leading to a greater-than-2 scaling in $t_{1/2}$ with s. Nonetheless, doubling the spacer length s from 10 to 20 indeed roughly quadruples $t_{1/2}$. Another reason is that, due to the finite sticker size, some small fraction of the stickers already overlaps at the point of quench.

For small spacer length $s \sim M$, the reaction can occur during the compact exploration ($\delta R \sim t^{1/3}$) before the spacers thermalize. The point for $s=5$ in Fig. 4 therefore suggests DC kinetics for this relatively smaller spacer size. We did not, however, conduct simulations at other, lower spacer lengths ($s \ll M$), where we again expect MF kinetics due to initial overlaps of stickers. Future simulation work will be devoted to a better understanding of DC kinetics alone.

The EB regime is also apparent from our simulations. Figure 5 shows results from an example collapse for $s=20$, which illustrates barrier-mediated kinetics. Figure 5(a) shows the potential energy of AA contacts per A-type monomer ($A=$''side-chain'' type), U_{aa}, and the collective squared radius of gyration of all side-chain monomers, $R^2_{g,aa}$. Clearly, $R^2_{g,aa}$ does not faithfully reveal the mechanism of the collapse when compared to U_{aa}, which shows clear transitions from plateau to plateau as micelles combine. Snapshots of representative conformations from each of the plateau regions labeled in Fig. 5(a) appear in Fig. 5(b). Various

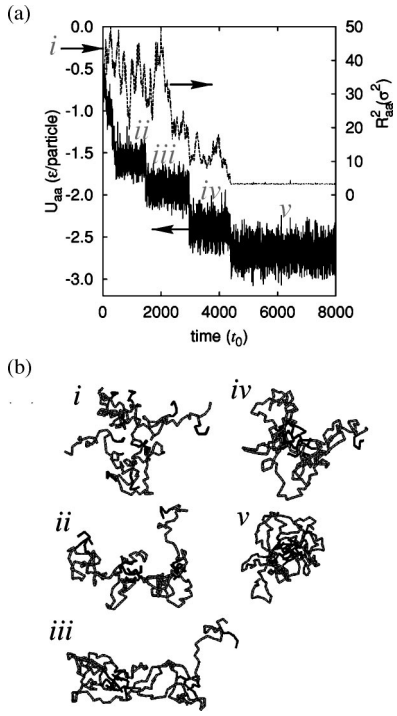

FIG. 5. (a) Side-chain collective squared radius of gyration, $R^2_{g,aa}(t)$, side-chain/side-chain monomer-monomer potential energy $U_{aa}(t)$ after solvent quench at $t=0$ for a particular simulation of a molecule of ten side chains with $M=5$ and $s=20$. Time is measured in units of t_0. The simulation domain contained 50 000 solvent particles in addition to the single polysoap molecule. The well-defined plateaus [labeled (ii)–(iv)] in $U_{aa}(t)$ identify intermediate metastable states consisting of several micelles each with $p < p^*$. (b) Snapshots of initial conformation (i), and representative conformations from the plateau regions identified in part (a). Side chains are black, and backbones are gray, and only bonds are rendered.

modes of aggregation are observed in this trajectory, including the merging of a $p=2$ and a $p=4$ cluster from state (ii) to (iii) and the merging of a single side chain into a $p=9$ cluster in the transition from (iv) to (v) to form the final micelle.

For the time scale of the collapse in the EB regime, we obtain from Eq. (19) $t \approx \frac{2}{3}(e^p)^{3/2}$, indicating logarithmic decay of $n_1(t)=\ln(\frac{2}{3})-\frac{3}{2}\ln(t)$. This logarithmic decay of $n_1(t)$ is indeed observed in the simulations, as depicted in Fig. 3(a). For both $s=10$ and 20, $n_1(t)$ clearly shows logarithmic scaling at late times $t>100t_0$, but it is difficult to pinpoint an exact crossover time into this regime. The picture becomes slightly clearer if we consider the decay of the total number of clusters, $n_t(t)$, computed from the simulations and shown in Fig. 3(b). It is evident that the onset of logarithmic scaling happens both sooner and for conformations with a larger number of clusters for $s=20$ relative to $s=10$. Longer spacer chains mean an earlier transition into energy-barrier-dominated kinetics, as predicted by the theory [Eq. (15)].

With current simulation range, the equilibrium state of polysoap is always a single cluster; therefore, we do not cover the slow collective mode. However, in the limit of the large spacer and large number of repeating units, sometimes the cluster size distribution can be kinetically trapped below p^*. Indeed, we observed several $s=20$ simulations that did

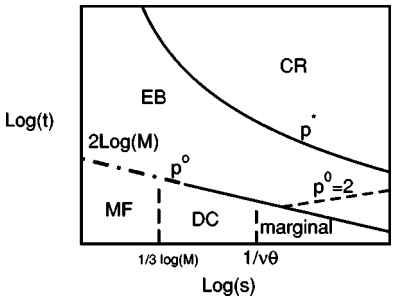

FIG. 6. The kinetic phases of polysoap cluster growth as a function of spacer size s and time t.

not fully collapse even after $\approx 25\,000 t_0$. Hence, the mean collapse time reported for $s=20$ in Table II is a lower bound.

V. DISCUSSION: THE KINETIC PHASE DIAGRAM

We now present a kinetic phase diagram for polysoap collapse in terms of the collapse time t and the hydrophilic backbone spacer length s in Fig. 6. The overlap aggregation number p^o divides short-time DC kinetics from long-time EB kinetics. The optimal micelle size p^* then divides EB from the slower CR kinetics. For short times and spacer lengths greater than side-chain lengths, marginal kinetics dominates. For a short chain with a few stickers, $N/s < p^o$, all side chains can combine pairwise following the marginal kinetics described in Sec. III A. The time for each step in the coarse graining remains the same, $\sim 1/k^{\mathrm{M}}$, until $p(t)$ becomes p^o. The dominant kinetic path is the repeated aggregation of two clusters of sizes p_1 and p_2, until all side chains are merged into a single cluster. To finish the collapse, the process should repeat $n_{cg}=\ln(N/2s)$ times. The total time for collapse is the sum of reaction times: $t_c = n_{cg} t_{1/2} = \ln(N/2s) s^{\nu(s+\theta_a)}$. The crossover from the early stage to the later stage (Daoud-Cotton regime) is given by the overlap concentration p^o for small spacer. For larger spacer, the energy barrier is relevant including the early kinetics. The dashed marginal-EB line indicates the time for cyclization $[p(t)=p^o=2]$.

After the average cluster size reaches p^*, the mass redistribution between clusters can be reached via exchanging single-side-chain clusters (CR). The line splitting marginal and EB is $t_{EB} \sim p^o/k^{\mathrm{M}} \sim s^{\mu} M^2$ and the slope in a log-log plot is the exponent $\mu=[(d+\theta)-6]\nu$. The y intercept indicates M dependence. The line between EB and CR is defined by $\ln(t) \sim p(t) \sim M^{4/5}/[3/5\ln(s)-1/3\ln(M)+\mathrm{const}]^{6/5}$.

VI. CONCLUSIONS

We have presented a theoretical kinetic phase diagram and simulations of the selective-solvent-induced collapse of polysoap molecules to form intramolecular micelles. The early stages are dominated by *marginal* first-order kinetics when the side chains are significantly shorter than the backbone spacers. As the cluster size grows, the rate of cluster coalescence becomes dominated by barrier-limited kinetics. For a long chain, the relaxation into the equilibrium state is a very slow process involving a collective relaxation of several established micelles. Results from large-scale molecular dynamics simulations of generic bead-spring polysoaps in explicit solvent corroborate the theory in three regimes (MF/DC and EB) of relatively short chains.

The polysoap is a well characterized heteropolymer and its sequence information is relatively simple compared to that of protein or other random heteropolymers. The kinetic properties are clearly attributed to the geometric construction and the ratio between the hydrophobic and hydrophilic monomers. Nonetheless, the kinetic phase diagram reveals several guiding principles in the dynamics of collapse transition of heteropolymers comprising spaced stickers which should prove useful in developing more complete kinetic theories of folding transitions of more complex macromolecules.

APPENDIX A: CONTACT EXPONENTS

Contact exponents were introduced by des Cloizeux for the contact probability between points of a single chain.[36,37] The contact probability that two extremities of a segment inside a single chain are at a relative distance x is

$$P_a(x) \sim (R)^{-d} F_a(x/R), \tag{A1}$$

with the scale R being the swollen size of the segment. $F(z)$ is a universal function which depends on the location of the considered segment along the chain:

$$F_a(z) \sim z^{\theta_a} (z \to 0), \quad a=0,1,2. \tag{A2}$$

The des Cloizeaux contact exponent θ_a distinguishes three different pair types shown in Fig. 7. By convention, $a=0$ corresponds to the two extremities of a chain $a=1$ to the contact of one extremity inside the chain and $a=2$ to that of the internal points. The larger exponent for the internal points is due to the excluded volume effect.

APPENDIX B: LARGER STICKERS

1. Diffusion-controlled kinetics for larger stickers

We now must quantify ''sticker size'' in a meaningful way to discuss its effect on the collapse kinetics for those cases when the side-chain lengths are close to the spacer lengths. One possibility is to assume that the quench is sufficiently deep such that the side chains of length M collapse immediately into spherical stickers of size $M^{1/3}$ *prior* to aggregating [Fig. 1(b)]. If this were true, we would expect to be able to assume marginal kinetics when $s^{\nu} \gg M^{1/3}$; that is, when the size of the spacer chain is much greater than the size of a *self-collapsed* side chain. We would need to describe a different kinetic regime (so far not discussed here) for relatively shorter spacers. However, for the relatively short side chains (i.e., a few persistence lengths,) such full collapse is not to be expected except for extremely deep quenches. Our simulations indicate that at the chosen quench depth, individual side chains ($M=5$) fluctuate between open and collapsed conformations. Nevertheless the aggregated clusters of more than two side chains form a stable aggregate and micellization is always assured.

The main consequence is that, due to the fact that some side chains are open and effectively larger, the collapse kinetics are faster when compared with kinetics for pointlike

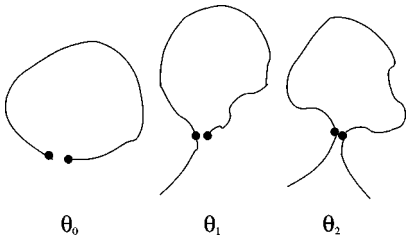

FIG. 7. des Cloizeaux's contact exponent: θ_0, θ_1, and θ_2 correspond, respectively, to the contact of two extremities of a chain ($a=0$), to the contact of one extremity inside the chain ($a=1$), and to that of the internal points ($a=2$).

stickers for the same spacer length s. A reaction can happen *before* the grafting points diffuse by a distance of s^{ν}, i.e., prior to spacer relaxation. The presence of fluctuating side chains yields a collapse process with three main types of reactions, illustrated in Fig. 8: (a) Collapsed sticker pairs which can be approximated as pointlike, (b) open and collapsed sticker pairs, and (c) open sticker pairs. As argued in the preceding section, the kinetics of the type-(a) reactions is marginal. If the quench is deep, the probability to have an open side-chain sticker is small. Thus, the reaction probability between pairs of open stickers is also rare. If the quench is shallow, weak interactions would not lead two open stickers to an irreversible aggregation. The ''open-open'' aggregation mechanism is therefore not considered here. We instead consider the open-closed reactions, which provide an additional kinetic mode which we term DC.

When the sticker size M is comparable to the spacer size s, due to the finite volume spanned by an open sticker, an open sticker has a chance to find a collapsed sticker prior to spacer relaxation if the distance between the grafting points is within the range of the sticker size. It now becomes important to calculate the size of the open sticker and the volume explored by it.

Consider a partially open sticker of size M', where $M' \leqslant M$. This conformation has a finite probability $\sim \tau^2 \exp(-M'\tau^2)$, where $\tau(\leqslant 1)$ is the depth of the solvent quench. The open chain of M' monomers is in an activated state. As we cannot think of any bias in the way they are generated, we assume Gaussian statistics. Such a bias could be that self-contacts accelerate the collapse and reduce the lifetime, but there was no clear evidence of such an effect in our previous single-chain collapse simulation.[12] The open sticker returns to the collapsed conformation after a typical collapse time $t_{coll} \sim M'/\tau^{12}$. The volume visited by an open sticker $V_{sausage}$ can be represented as a ''sausage'' of dynamical blobs of radius $\sim t^{1/3}$. Each of this blob is correlated and its exploration by the monomers is marginally dense. The volume explored by the open sticker is thus the total volume of the dynamic blobs $V_{sausage} \sim M' t^{1/3}$. The largest volume of the sausage before collapse is therefore $M' t_{coll}^{1/3}$, and the corresponding radius of the dynamic blob is the collapsed globule radius.[38] The probability for an open sticker to find a compact sticker is proportional to the ratio of the volume defined by the spacer size ($\sim s^{d\nu}$) to the actual volume visited by the open sticker $V_{sausage}$ before the collapse. The kinetic constant k^{DC} is proportional to the probability of making contact per unit time, the characteristic time being t_{coll}. We obtain this by integrating over all possible sticker sizes M' with their statistical weight and integrating over the volume the open sticker visits after dividing by the characteristic time t_{coll} for an open length M':

$$k_{\text{pair}}^{DC} = \int_0^M dM' t_{coll}^{-1} \tau^2 e^{-M'\tau^2} \frac{M'(M'/\tau)^{1/3}}{s^{d\nu}} \left(\frac{(M')^{1/2}}{s^{\nu}} \right)^{\theta_a}. \tag{B1}$$

Because of the activation barrier against opening the sticker (exponential factor under the integral), the main contribution to the integral is obtained when the open sticker size is $M' \sim 1/\tau^2$, leading to

$$k_{\text{pair}}^{DC} \sim \tau^{-\theta_a} s^{-\nu(d+\theta_a)}. \tag{B2}$$

For weak stickers, $r_{sticker}$ is larger but similar to b/τ and the open sticker channel contribution provides a correction to that of the closed sticker channel. The contact exponent θ_a does not play a role if the size of the partially open sticker is as large as the spacer size ($b/\tau \sim s^{\nu}$) where the probability to be in the reaction range is of order unity. We obtain the kinetic constant k_{DC} as

$$k_{\text{pair}}^{DC} \sim s^{-d\nu}. \tag{B3}$$

We note that in order to bring the sticker to the collapsed size, τ should be at least as large as $1/\sqrt{M}$ which provides the upper bound of the kinetic constant k^{DC}. In the limit of $\tau \to 1$, the strong sticker regime [described in Eqs. (6) and (7)], stickers can be approximated as pointlike. For smaller $\tau < 1$, fluctuations are important (provided $M\tau^2$ is not much larger than one) and the volume spanned by the open sticker is relevant. If the size of the partially open sticker (typically a few thermal blobs) is larger than both the spacer size and the collapsed globule, the fluctuation covers all ranges of possible contact, so the contact exponent does not contribute to the kinetic rate. Open stickers then dominate the kinetics. In this regime we cannot expect sticker pair dissociation to be completely negligible.

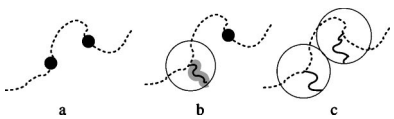

FIG. 8. Schematic illustrations of sticker pair types: (a) two collapsed stickers; (b) open and closed stickers; and (c) two open stickers. The gray region indicates the volume visited by compact exploration.

2. Overlapping stickers: MF kinetics

If side chains are very large compared to spacers ($M > s$), the side chains are initially overlapping. The early-stage kinetics is described by MF based on the chain conformation before the solvent quench, in the sense that the prequench conformations represent a statistical ensemble of sticker-pair distribution functions.

As already mentioned, from our previous single homopolymer chain collapse study,[12] self-contacts do not seem to play any essential role in the kinetics at least at the scaling level. It is thus likely, yet not proven, that single sticker

collapse driven by internal tension prevails on joint collapse with many crosslinks (in the absence of entanglements) at least for deep quench where the collapse is strongly deterministic. The initially overlapping prequench conformations may nonetheless form a small stable preglobule built upon a contact point (there are initially of order 1 contact points). This initial MF regime with a reaction rate $Q \sim \tau^3$ crosslinks the two side chains after the relaxation time of a thermal blob. Further collapse will proceed by a streamlining and final collapse process, as is the case for an isolated homopolymer chain, and the soluble main chain exerts only a negligible force opposing collapse. The final collapse directed by the tension $\sim\tau$ occurs over a distance $\sim r_s \sim s^\nu$ with a friction $\sim r_s$ dominated by the spacer. The associated terminal time thus reads $s^{2\nu}/\tau$.

ACKNOWLEDGMENTS

C.F.A. acknowledges Drexel University for startup funds. The authors are grateful to S. Obukhov and A. Johner for insightful comments and suggestions and careful reading of our manuscript.

[1] P. G. de Gennes, J. Phys. (France) Lett. **46**, L639 (1985).
[2] A. Y. Grosberg and D. Kuznetsov, Macromolecules **26**, 4249 (1993).
[3] Y. A. Kuznetsov, E. Timoshenko, and K. Dawson, J. Chem. Phys. **103**, 4807 (1995).
[4] A. Buguin, F. Brochard-Wyart, and P. G. de Gennes, C. R. Acad. Sci., Ser. IIb: Mec., Phys., Chim., Astron. **322**, 741 (1996).
[5] V. Rostiashivili, N.-K. Lee, and T. Vilgis, J. Chem. Phys. **118**, 937 (2003).
[6] R. Chang and A. Yethiraj, J. Chem. Phys. **114**, 7688 (2001).
[7] A. Milchev and K. Binder, Europhys. Lett. **26**, 671 (1994).
[8] E. G. Timoshenko, Y. A. Kuznetsov, and K. A. Dawson, J. Chem. Phys. **102**, 1816 (1995).
[9] E. Pitard and H. Orland, Europhys. Lett. **41**, 467 (1998).
[10] B. Chu, Q. Ying, and A. Y. Grosberg, Macromolecules **28**, 180 (1995).
[11] C. Wu and S. Zhou, Phys. Rev. Lett. **77**, 3053 (1996).
[12] C. F. Abrams, N.-K. Lee, and S. Obukhov, Europhys. Lett. **59**, 391 (2002).
[13] S. Hagen, J. Hofrichter, A. Szabo, and E. W. A., Proc. Natl. Acad. Sci. U.S.A. **93**, 11615 (1996).
[14] L. Qiu, C. Zachariah, and S. J. Hagen, Phys. Rev. Lett. **90**, 168103 (2003).
[15] N.-K. Lee, A. Johner, and T. A. Vilgis, Macromolecules **35**, 6043 (2002).
[16] O. V. Borisov and A. Halperin, Langmuir **11**, 2911 (1995).
[17] A. Lashewki, Adv. Polym. Sci. **124**, 1 (1995).
[18] E. G. Timoshenko and Y. A. Kuznetsov, Colloids Surf., A **190**, 135 (2001).
[19] V. V. Vasilevskaya, A. A. Klochkov, P. G. Khalatur, A. R. Khokhlov, G. ten Brinke, Macromol. Theory Simul. **10**, 389 (2001).
[20] I. R. Cooke and D. R. M. Williams, Macromolecules **36**, 2149 (2003).
[21] J. D. Weeks, D. Chandler, and H. C. Andersen, J. Chem. Phys. **116**, 7244 (1971).
[22] J. Polson and M. J. Zuckermann, J. Chem. Phys. **116**, 7244 (2002).
[23] K. Kremer and G. S. Grest, J. Chem. Phys. **92**, 5057 (1990).
[24] C. F. Abrams and K. Kremer, J. Chem. Phys. **115**, 2776 (2001).
[25] M. Pütz and A. Kolb, Comput. Phys. Commun. **113**, 146 (1998).
[26] M. Daoud and J. P. Cotton, J. Phys. (Paris) **43**, 531 (1982).
[27] B. Friedman and B. O'Shaughnessy, Europhys. Lett. **21**, 779 (1993).
[28] B. O'Shaughnessy, in *Theoretical and Mathematical Models in Polymer Research,* edited by A. Y. Grosberg (Academic, San Diego, 1998).
[29] G. Wilemski and M. Fixman, J. Chem. Phys. **60**, 866 (1974).
[30] M. Doi, J. Chem. Phys. **79**, 5080 (1983).
[31] In Rouse dynamics, the friction is instead proportional to the correlated contour length; hence, the diffusion coefficient decreases as $D(t) \sim 1/\sqrt{t}$ for subchains with length $s'(t) < s$. The fluctuation of the mean-squared displacement is $\delta R(t) \sim t^{1/\alpha}$ with the kinetic exponent $\alpha = 4$. (Ref. 32). In this regime, the volume visited by the subchain is $\sim t^{3/4} < t$ in $d = 3$, previously denoted as ''compact exploration'' by de Gennes (Ref. 32).
[32] P. G. Gennes, J. Chem. Phys. **76**, 3316 (1982).
[33] In a good solvent, the field theoretic values using ϵ expansion report $\theta_0 = 41/128$, $\theta_1 = 29/64$, $\theta_2 = 17/32$. The trend is clear. As for the middle points, excluded volume effect reduces the probability to make contacts.
[34] The Daoud-Cotton model is restricted to true star geometries and presumably of order of 50 branches.
[35] A. Johner and J.-F. Joanny, Macromolecules **23**, 5299 (1990).
[36] B. Duplantier, J. Stat. Phys. **54**, 581 (1989).
[37] J. des Cloizeaux, Phys. Rev. A **10**, 1665 (1974).
[38] Strictly speaking the relevance of diffusive broadening through dynamic blobs is not obvious for the collapse of (large) strong stickers. If we follow Ref. 12, the streamlining process that aligns larger and larger chain sections under the effect of tension in a sense suppresses short scale fluctuations. On the other hand, the driving force is almost negligible for the few thermal blobs typically opened. Indeed the collapse time after Ref. 12 then merges with the relaxation time of thermal blob. This justifies the relevance of anomalous diffusion.